JACS
JOURNAL OF THE AMERICAN CHEMICAL SOCIETY
Article
pubs.acs.org/JACS

Hybrid Halide Perovskite Solar Cell Precursors: Colloidal Chemistry and Coordination Engineering behind Device Processing for High Efficiency

Keyou Yan,*[,†,‡,§] Mingzhu Long,[†,§] Tiankai Zhang,[†,§] Zhanhua Wei,[‡] Haining Chen,[‡] Shihe Yang,*[,‡] and Jianbin Xu*[,†]

[†]Department of Electronic Engineering, The Chinese University of Hong Kong, Shatin, New Territories, Hong Kong
[‡]Department of Chemistry, The Hong Kong University of Science and Technology, Clear Water Bay, Kowloon, Hong Kong

Supporting Information

ABSTRACT: The precursor of solution-processed perovskite thin films is one of the most central components for high-efficiency perovskite solar cells. We first present the crucial colloidal chemistry visualization of the perovskite precursor solution based on analytical spectra and reveal that perovskite precursor solutions for solar cells are generally colloidal dispersions in a mother solution, with a colloidal size up to the mesoscale, rather than real solutions. The colloid is made of a soft coordination complex in the form of a lead polyhalide framework between organic and inorganic components and can be structurally tuned by the coordination degree, thereby primarily determining the basic film coverage and morphology of deposited thin films. By utilizing coordination engineering, particularly through employing additional methylammonium halide over the stoichiometric ratio for tuning the coordination degree and mode in the initial colloidal solution, along with a thermal leaching for the selective release of excess methylammonium halides, we achieved full and even coverage, the preferential orientation, and high purity of planar perovskite thin films. We have also identified that excess organic component can reduce the colloidal size of and tune the morphology of the coordination framework in relation to final perovskite grains and partial chlorine substitution can accelerate the crystalline nucleation process of perovskite. This work demonstrates the important fundamental chemistry of perovskite precursors and provides genuine guidelines for accurately controlling the high quality of hybrid perovskite thin films without any impurity, thereby delivering efficient planar perovskite solar cells with a power conversion efficiency as high as 17% without distinct hysteresis owing to the high quality of perovskite thin films.

INTRODUCTION

Two basic recipes of 1:1 CH_3NH_3I/PbI_2 and 3:1 $CH_3NH_3I/PbCl_2$ have been widely employed among perovskite solar cells (PSCs) as starting precursor solutions to produce $CH_3NH_3PbI_3$ and $CH_3NH_3PbI_{3-x}Cl_x$ thin films separately.[1−10] As confirmed, $CH_3NH_3PbI_3$ perovskite has an about 100 nm diffusion length, whereas the negligible chlorine mixed counterpart $CH_3NH_3PbI_{3-x}Cl_x$ can afford a diffusion length as long as 1 μm in polycrystalline films.[11−14] Therefore, pristine $CH_3NH_3PbI_3$ needs to use a mesoporous TiO_2 film to assist film formation and electron collection for a high-efficiency PSC.[15,16] However, $CH_3NH_3PbI_{3-x}Cl_x$ can be directly deposited in a planar fashion with a power conversion efficiency (PCE) as high as 19.3%.[6,17] Despite the very similar crystalline structure of the perovskite phase, it is found that the 1:1 CH_3NH_3I/PbI_2 stoichiometric recipe produced large rodlike bundles in $CH_3NH_3PbI_3$ films in general conditions and thereby cannot be used to make high-quality films in a planar fashion.[2] This further drew great attention to perform effective solvent engineering for eliminating the undesired 1D morphology toward a flat film in the stoichiometric recipe, such as using mixed solvents (DMSO/GBL) and solvent treatment (toluene dribbling)[15] and deposition procedure optimization (e.g., two-step deposition or an assistance additive)[2,16,18−22] for film amelioration. Therefore, the perovskite precursor solution plays the central role in film quality and solar cell performance.[23−35] To date, however, a scientific investigation of the precursors themselves directly for solar cell implementation has not been fully conducted,[36,37] and fundamental insights into the perovskite precursor have not been well addressed yet.

Herein, we first present the crucial colloidal chemistry visualization of the perovskite precursor solution based on analytical spectra and reveal that perovskite precursor solutions are generally colloidal dispersions in a mother solution, rather than real solutions. The organic component not only acts as a reagent for solid-phase transformation to perovskite, but also plays a crucial role in coordination with the inorganic

Received: January 11, 2015
Published: March 17, 2015

DOI: 10.1021/jacs.5b00321
J. Am. Chem. Soc. 2015, 137, 4460−4468

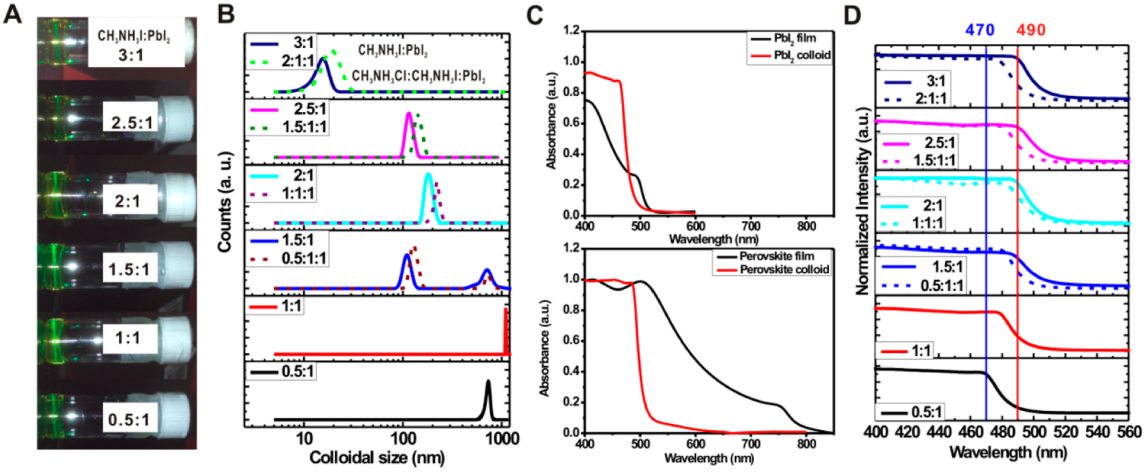

Figure 1. Colloidal properties of perovskite precursors at room temperature: (A) Tyndall effect photographs; (B) size distribution by dynamic light scattering; (C) UV spectra of colloids (red) and thin films (black) for PbI_2 (top) and perovskite (bottom); (D) UV spectra of perovskite precursors with different organic:inorganic component ratios.

component as the colloidal soft framework, and thereby, the coordination complex of organic−inorganic components actually determines the final perovskite quality (such as film morphology, grain size, and crystallinity). Undesired large 1D structures produced by the 1:1 CH_3NH_3I/PbI_2 recipe, which are rod-shaped colloids made of iodine coordination on the (001) edge of PbI_2 at first and transform to PbI_2-impure perovskite with reserved rod-shaped morphology, interfering in the formation of the pure and flat perovskite films, are effectively eliminated with the aid of the mechanistic understanding of colloidal formation and coordination engineering of the colloidal shape using excess methylammonium halides. Transformation from a precipitated precursor to perovskite with high coverage, aligned crystallography, and high purity is achieved gradually, enabling as high as 17% PCE in planar version PSCs, owing to judicious colloidal control, coordination engineering, and thermal leaching. The present study addresses the most important fundamental chemistry of the perovskite precursor and provides a genuine guideline for accurately controlling the thin-film quality of hybrid perovskite materials, leading to a meaningful scenario of the chemical reactions in terms of materials processing.

RESULTS AND DISCUSSION

Colloidal Pretest. The colloidal properties of the perovskite precursors are first identified by typical Tyndall effects. At first, perovskite precursors with different organic:inorganic ratios of CH_3NH_3I to PbI_2 or CH_3NH_3Cl/CH_3NH_3I to PbI_2 aiming at exhibiting colloidal tunability were prepared by sequential addition of PbI_2 stock solution and CH_3NH_3I (or CH_3NH_3Cl + CH_3NH_3I) into dimethylformamide (DMF) solution and subjected to 30 min of ultrasonic dispersion and 4 h of vigorous stirring. Figure S1 (Supporting Information) shows photographs of the basic precursor solutions at different ratios of CH_3NH_3I to PbI_2, which are absolutely yellow and transparent to the naked eye (Figure S1A). However, as shown in Figure 1A (also in Figure S1B,C), we can see all the solutions display a typical Tyndall effect; that is, with a green laser to pass through the solution, the light beam can be observed, which means that such solutions are colloidal dispersions in the mesoscale, not real solutions. To confirm the colloidal attributes and assess the colloidal tunability in more detail by ratio control, dynamic light scattering was further employed to verify the size distribution of the dispersion in the precursor solutions. Generally, the dispersed-phase compounds with different component ratios have a diameter between approximately 10 and 1100 nm (see Figure 1B), which confirms that all the solutions are well-defined colloids. Specifically, the colloidal size is changed with different loadings of the organic component. First, the size of the colloidal particles in a 0.5:1 ratio distributes at a peak of 740 nm, with that of the 1:1 ratio increasing to 1097 nm. Second, the 1.5:1 ratio has two size distribution peaks at around 109 and 740 nm. Third, the sizes of the 2:1 and 2.5:1 ratios decrease to about 200 nm with further loading of organic component, and the 3:1 ratio even has a size down to 16.5 nm. In addition, the replacement of the excess part of stoichiometric CH_3NH_3I (CH_3NH_3I coordination engineering) by using CH_3NH_3Cl (CH_3NH_3Cl coordination engineering) in this system herein not only induces a little larger size of the colloid than that of pure CH_3NH_3I but will also play a crucial role in the film purity hereafter due to facilitating nucleation and impurity leaching, which will be discussed in the following. Besides, it is noted that the size measured for the 3:1 and 2:1:1 combinations is consistent with the previous result for 3:1 $CH_3NH_3I/PbCl_2$ by cryo-TEM (about 10 nm) and thereby can be regarded as direct evidence of the colloid.[37]

Colloidal Structure. For an explanation of the size distribution, ultraviolet−visible (UV) spectroscopy was further used to detect structural information on the precursor solutions. First, we compared the absorption difference between the colloids and their corresponding thin films. As shown in the top panel of Figure 1C, the colloid has a significant blue shift of absorption compared to thin films, which can be easily explained by the reduced size or partial dissolution effect in the solution. More interestingly, the perovskite colloidal precursor has a much more red shifted plateau absorption edge (490 nm) than the pure PbI_2 colloid (460 nm) (bottom panel of Figure 1C), which suggests that the perovskite precursor is made of not only PbI_2 and CH_3NH_3X (X = Cl, I, Br) dissolved in DMF, but also primarily a series of new coordination compounds. Moreover, different from thin films, the colloidal compounds have a representative absorption plateau in the wide spectral range, which is probably caused by

DOI: 10.1021/jacs.5b00321
J. Am. Chem. Soc. 2015, 137, 4460−4468

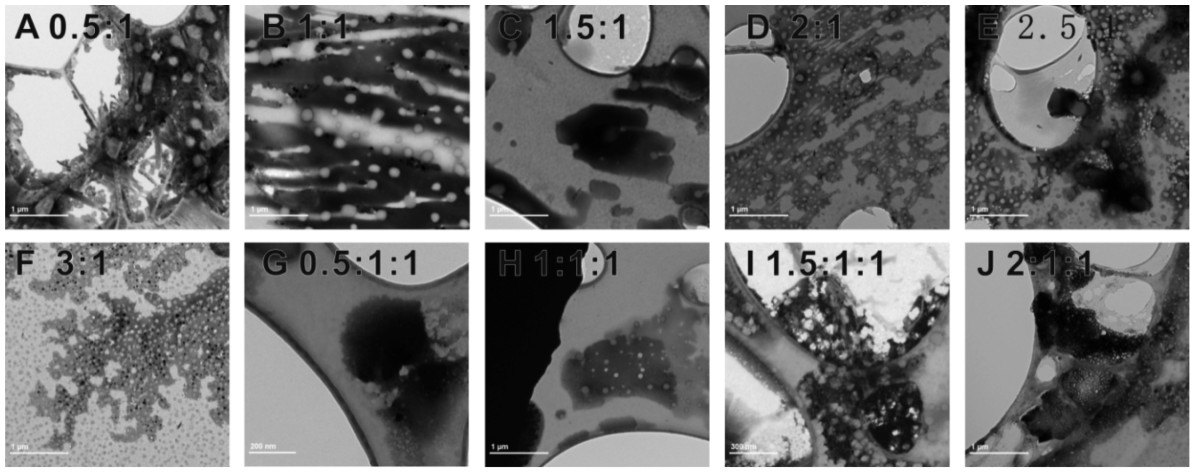

Figure 2. Wet-TEM images for early observation of the colloidal soft framework in different component precursors: (from A to J) 0.5:1, 1:1, 1.5:1, 2:1, 2.5:1, and 3:1 CH_3NH_3I/PbI_2 and 0.5:1:1, 1:1:1, 1.5:1:1, and 2:1:1 $CH_3NH_3Cl/CH_3NH_3I/PbI_2$.

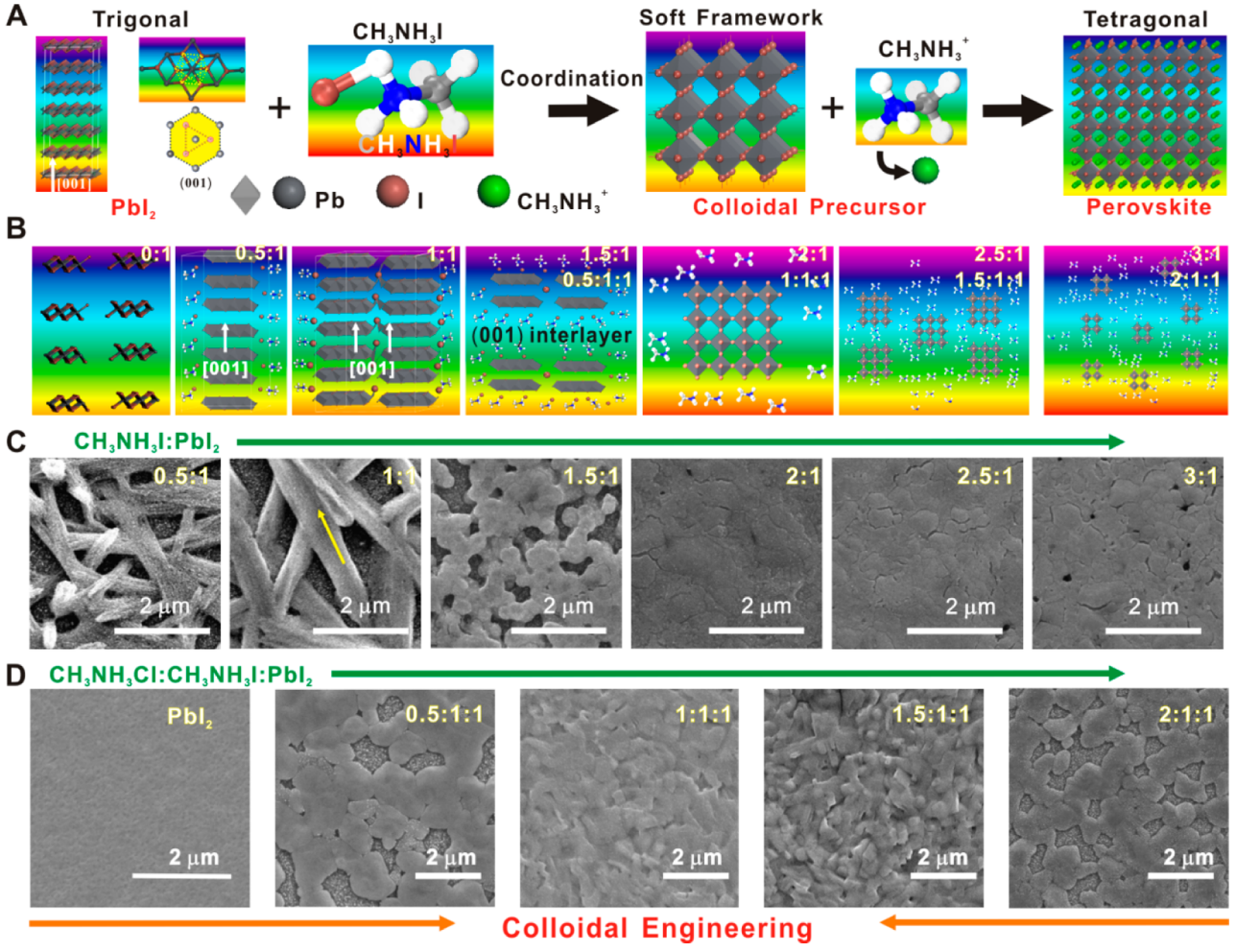

Figure 3. Colloidal chemistry and coordination engineering: (A) Schematic illustration of the colloidal intermediate phase in the solution of perovskite from starting material (PbI_2 + CH_3NH_3I → soft coordination colloid → $CH_3NH_3PbI_3$, which is actually a corner-shared octahedral soft framework (denoted as $[-PbI_x-...-PbI_x-]_n$), and CH_3NH_3 is not sterically arranged in a lattice at this stage due to its higher solubility) (also see Figure S2, Supporting Information). (B) Possible organic−inorganic coordination products at different levels with different contents of organic compound in perovskite precursors. (C) Supporting SEM micrographs of calcined thin films with CH_3NH_3I coordination engineering. (D) Supporting SEM micrographs of the final perovskites with optimized film morphology by CH_3NH_3Cl coordination engineering.

coordination equilibrium between colloids at different coordination levels. Namely, the absorption features of series of compounds with different coordination states will overlap as absorption plateaus in the coordination systems. On the basis of coordination chemistry, coordination complexes can be made of a variety of lead polyiodides, such as $[PbI_3]^{1-}$,

DOI: 10.1021/jacs.5b00321
J. Am. Chem. Soc. 2015, 137, 4460−4468

$[PbI_4]^{2-}$, $[PbI_5]^{3-}$, and $[PbI_6]^{4-}$. Obviously, $[PbI_6]^{4-}$ is the full coordination compound, with a free octahedral structure, and the other lower coordination levels of complexes tend to share halogen ions in the form of corner-sharing for full coordination, resulting in a soft framework toward the colloidal range (see Figure S2 (Supporting Information) for details). Therefore, the CH_3NH_3X:PbI_2 ratio will play an important role in the halogen-sharing degree, further determining the colloid size. Figure 1D displays the UV spectra for all the colloidal precursors. It is seen that an organic:inorganic ratio larger than 1.5:1 has a similar excitonic absorption plateau edge at 490 nm probably due to full coordination through atom sharing, but a ratio of less than 1.5:1 cannot ensure enough coordination from the distinct blue shift versus 490 nm (absorption plateau edge of full coordination). Besides, although the excess of organic component at a 1.5:1 ratio is much larger than that at a 1:1 stoichiometric ratio, the absorption plateau edge is just close to 490 nm, indicating that full coordination will be realized with excess organic component. This absorption feature can be associated with two size distribution peaks of the 1.5:1 ratio, which also arise from the nearly full coordination complex colloid and PbI_2-rich colloid with limited coordination with iodine ions, respectively. To interpret more convincingly that the perovskite colloid is really made of the coordination complex, the excess of CH_3NH_3I over the stoichiometric ratio is replaced by CH_3NH_3Cl as previously mentioned, which should form a possible mixed coordination compound (e.g., $[PbI_{6-x}Cl_x]^{4-}$), leading to tuning the band gap of the colloidal compound for the observation of coordination. As expected, the absorption band edge is indeed blue shifted and gradually shifted by increasing the content of CH_3NH_3Cl (Figure 1D, dashed lines), indicating the formation of a mixed halide coordination compound in the system. Moreover, the coordination compound at different ratios can be sophisticatedly judged from the colors of the precursor thin films (Figure S3A, Supporting Information), which are actually aggregations of the coordination complex with different transformation extents to the perovskite phase depending on the CH_3NH_3I amount after solvent removal. For example, more CH_3NH_3I permits less I sharing between coordination complexes and induces smaller soft framework units, leading to a lower transformation extent toward perovskite due to the separation effect by CH_3NH_3I termination between soft framework units; thereby, the precursor films display colors more similar to that of the precursor solution than that of the perovskite film (see Figure S3A, 3:1; it is indeed yellow but not black).

To provide earlier visible information on the colloids, wet-TEM was further performed, which allows partial observation of the precipitation of the colloids conveniently. Figure 2 shows that all the colloids are generally made of a soft framework as expected. Generally, in line with previous dynamic light scattering results, 0.5:1 and especially 1:1 have a larger size than the others with a rod-shaped top structure, which were still made of an amorphous framework inlaid with nanoparticles. In the CH_3NH_3I-rich systems (1.5:1, 2:1, 2.5:1, 3:1), the amount of 1D structure decreases and the morphology gradually turns to a hollow framework, which can be regarded as interweaved networks of partially iodine-shared octahedra of a lead polyiodide framework. Especially in the chlorine involved system, the size of the framework is a little larger than that of the corresponding CH_3NH_3I-rich counterpart (such as 3:1 vs 2:1:1), which means that the chlorine addition accelerates the crystalline nucleation process. Therefore, one can see that more nanoparticles have appeared inside the framework, which have been assigned to $PbCl_2$ nuclei in a previous study.[37]

Colloidal Formation. We deduce the formation of the colloid in precursors more clearly and correlate it to subsequent morphologies of the thin films by resorting to geometrical crystallography and building the model for further discussion on the structure transformation from PbI_2 to perovskite. As schematized in Figure 3A, PbI_2 tends to crystallize in the trigonal $P\bar{3}m1$ space group, with stacked (001) planes along the *c*-axis direction through van der Waals force and dangling bonds at the (001) edges, which would allow facile insertion of guest molecules (such as DMF) into the interlayer space for coordination and dissolution, while $CH_3NH_3PbI_3$ has a tetragonal perovskite structure phase of the *I*4/*mcm* space group at room temperature. Hence, the transformation from PbI_2 to $CH_3NH_3PbI_3$ should first form a soft coordination framework (Figure 3A, middle) as an intermediate phase toward a tetragonal scaffold. From the above colloidal Tyndall effect and dynamic light scattering, the formation of the soft framework is completed in the solution. In the following, we will interpret the film morphologies with different precursor ratios in more detail correlated to different coordination degrees and modes, as schematically depicted in Figure 3B, with corroborative evidence from SEM images of the final films in Figure 3C,D. When PbI_2 is dissolved in DMF solution, PbI_2 species first fall into (001)-aligned pieces due to facile breakdown of van der Waals interaction between (001) interlayers and are then coordinated with DMF to break some chemical bonds inside the (001) intralayer for full dissolution. After the initial introduction of CH_3NH_3I into PbI_2 solution, PbI_2 is prone to precipitation due to the dissolution competition with CH_3NH_3I. It is CH_3NH_3I that will selectively coordinate with PbI_2 at (001) plane edges at first due to dangling bonds at these sites. Therefore, such selective coordination modes allow CH_3NH_3I to serve as a surfactant at this stage to form colloidal PbI_2 nanorods abiding by trigonal crystallography of PbI_2 and further string the (001) plane stacked nanorods together in the form of nanorod bundles through the atom sharing of halogen between nanorods, as schematized in Figure 3B and evidenced in Figure 3C (see 0.5:1, small bundles, and 1:1, ultralarge bundles). After a slight increase in the content of the organic component, the CH_3NH_3I solution will become a solvent to dissolve and coordinate the back-precipitated trigonal PbI_2 colloid toward a tetragonal transformation for maximum coordination, and thereby, the 1D morphology will greatly decrease (Figure 3C, 1.5:1 CH_3NH_3I/PbI_2) and even disappear and hexagonal disk slices will become observable (see Figures S4 and S5 (Supporting Information) and Figure 3D, 0.5:1:1 $CH_3NH_3Cl/CH_3NH_3I/PbI_2$), which is a scenario of intercalation of guest CH_3NH_3I (or CH_3NH_3Cl) lodged in the PbI_2 (001) host interlayers in 1D rods (schematized in Figure 3B, 1.5:1, 0.5:1:1) by coordination reaction. A further increase in the content of the organic component will enter into the nonselective coordination mode and build a quasi-tetragonal soft framework (Figure 3A, middle, colloidal precursor), which consists of three spatially corner-sharing octahedral coordination complexes (see Figure S2 (Supporting Information)), and the morphology of continuous films is formed afterward, as expected by subsequent crystallization (Figure 3C,D, 2:1, 1:1:1). A higher content of organic component (2.5:1, 3:1) will decrease the colloidal size in the solution (Figure 3B, 2.5:1,

DOI: 10.1021/jacs.5b00321
J. Am. Chem. Soc. 2015, 137, 4460−4468

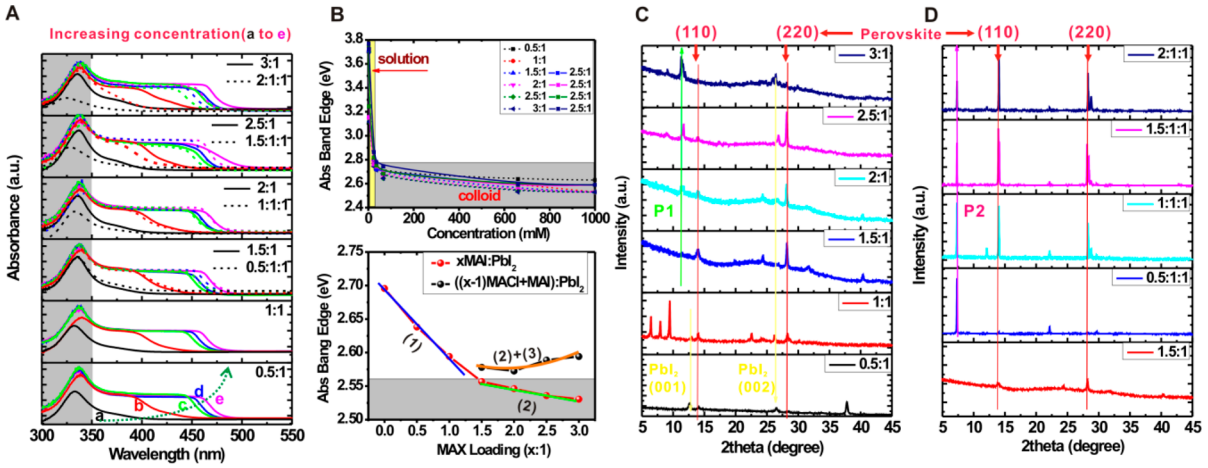

Figure 4. Evolution of the precursor: (A) concentration-induced precursor transformation from solution to colloid (curve a, solution (1 mM); curves b–e, colloids (3, 24, 35, and 66 mM)); (B) concentration dependence (top) of the coordination complex and its composition effect (bottom) in colloidal absorption of the precursor; (C) XRD of the precursor film by CH_3NH_3I coordination engineering; (D) XRD of the precursor film by CH_3NH_3Cl coordination engineering.

1.5:1:1) and yield smaller perovskite crystals in the thin films (Figures 3C,D, 2.5:1, 1.5:1:1), because less atom sharing among $[PbX_6]$ octahedra will separate coordination units and induce a smaller colloidal framework (Figure 1B, 3:1), or even individual octahedral units, leaving some organic residue (see Figure 3C, 3:1) or a much greater boundary gap (Figure 3D, 2:1:1) in the perovskite films after removal of the excessive organic component.

Influential Parameters of the Colloid. After confirmation of the colloid, we discuss some parameters in relation to colloidal behaviors. Temperature is an important parameter for pure PbI_2 colloids, which require higher temperature (70 °C) to dissolve fluffy precipitates into colloid for better film deposition.[2] We found in our systems that, due to the addition of CH_3NH_3I, the solubility of PbI_2 increases a lot since there is no precipitate at room temperature, which can be related to the iodine coordination of Pb^{2+}. Therefore, the amount of CH_3NH_3X is a more important parameter than temperature in our systems, as discussed above.

We also investigated the concentration effect on the colloidal behaviors, which we found was a very important parameter in our systems. Concentrations of 1, 3, 24, 35, and 66 mM were further prepared and then subjected to optical absorption measurement (Figure 4A). A concentration lower than 1 mM displays real solution behavior (Figure 4A, black line), with an absorption peak at about 330 nm (PbI_2 monomer), an absorption feature at 370 nm ($[PbI_3]^{1-}$), and an absorption band edge at 425 nm($[PbI_4]^{2-}$),[36] with a small blue shift after excess addition of CH_3NH_3Cl. However, a little higher concentration will induce an absorption transformation from a solution feature (without an absorption plateau) to a colloidal feature (with an absorption plateau) as discussed before in association with a red-shifted absorption edge, indicating a shift of equilibrium toward colloidal compounds. To summarize the concentration dependence, we plot the absorption plateau edge versus concentration (Figure 4B, top) and find that the transformation from solution to colloid exhibits threshold behavior (critical concentration),[38] that is, an abrupt change from solution to colloid with respect to concentration. With the addition of CH_3NH_3Cl, the colloidal absorption edge becomes more stable judging from the more flat curves (see solid curves in Figure 4B, top) and thus larger colloid (see above Figure 1B), which is probably related to chlorine-induced nucleation, in support of the soft framework.[37] Therefore, CH_3NH_3Cl engineering can lead to a stable colloidal system. On the basis of the concentration effect on the dispersion properties, we can conclude that the colloid is made of a colloidal intermediate lead polyhalide framework through halogen sharing dispersed in a mother solution.

In addition, we revisited the composition effect on the colloidal behavior. Three trend lines are labeled in Figure 4B, bottom. The first linear region (1) indicates the coordination reaction happens. A slight stoichiometric excess (intercept at 1.4:1 CH_3NH_3I/PbI_2) of CH_3NH_3I suggests that excess organic component can also serve as a solubilizer of PbI_2 in this system, which is consistent with its higher solubility than that of pure PbI_2–DMF solution and also infers that the colloid framework is dispersed in the organic–inorganic mother solution.[34] In the second linear region (2), the solubilizer role of CH_3NH_3I will be played more and more in reduction of the colloidal size as the preceding discussion for Figure 1B. The third nonlinear curve in the CH_3NH_3Cl addition system indicates that there exist multiple processes, which are assigned to one similar to that of (2) and another one (3) related to $PbCl_2$ nucleation in combination with the band gap bowing effect of $PbI_{2-x}Cl_x$[39,40] and so on.

Colloid-Based Perovskite Growth. To trace further transformation from the colloid to perovskite, we first perform XRD for the perovskite precursor films aforementioned. Parts C and D of Figure 4 show the XRD patterns of precursor films using CH_3NH_3I and CH_3NH_3Cl engineering, respectively. In CH_3NH_3I engineering, although $CH_3NH_3PbI_3$ is weakly observable from the (110) and (220) peaks at 14.12°, and 28.44°, respectively, the films still display a much more amorphous feature of the coordination complex from the large bump distributed in a wide range (2θ) (Figure 4C). However, in CH_3NH_3Cl engineering, instead, high-intensity narrower peaks indicative of the (110) and (220) lattice planes are remarkable, along with a strong small-angle peak at 7.5°, probably in correlation to large interplanar spacing (d = 0.154/(2 sin θ) = 3.75 nm) of a chlorine-coordinated mesoscopically layered intermediate phase. On the basis of an additional peak at 7.5° and its reduced intensity with respect to increased CH_3NH_3Cl content (see Figure 4D), we infer that the

DOI: 10.1021/jacs.5b00321
J. Am. Chem. Soc. 2015, 137, 4460–4468

perovskite species crystallizes with aligned orientation and allows chlorine to selectively occupy the apex of the octahedron when a small amount of CH_3NH_3Cl is loaded,[41] which is supported by the perovskite sheet morphology (Figure 3D) and the absence of the peak at 7.5° after CH_3NH_3Cl release (Figure 6B).[19] At least the appearance of a well-defined perovskite phase in the precursor film once again suggests that chlorine accelerates the nucleation process, at first yielding a large colloidal size in the mother solution (Figure 1B) and rendering larger crystalline grains in the final films (see Figure 3C,D, 0.5:1:1 vs 1.5:1).

From the previous concentration dependence, the perovskite precursor should be made of colloids dispersed in a mother solution. To demonstrate the colloid plays a more important role in the morphology of the final perovskite than the mother solution, we check the top morphology of the film and bottom grain of perovskite with a longer calcination time for the complete transformation from precursor to perovskite through interdiffusion[42,43] (thermal leaching and additional 20 min of tempering with a coverslip atop). For simplification, here we only use 1:1 and 0.5:1:1 with and without large rod-bundle top structures separately for demonstration. Parts A and B of Figure 5 show the rod-shaped top structure with a large bottom

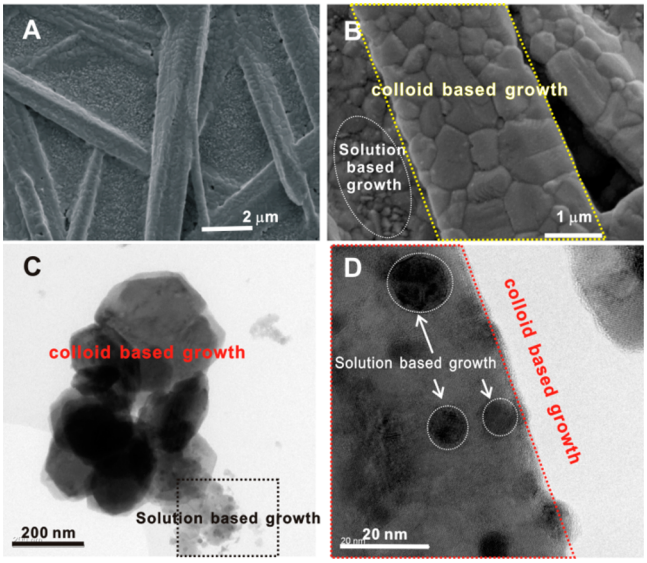

Figure 5. Solution- versus colloid-based growth demonstration: (A) SEM and (B) HRSEM of the perovskite film using the 1:1 recipe; (C) TEM and (D) HRTEM using the 0.5:1:1 recipe.

perovskite grain inlaid in the rod and small perovskite grains also deposited on the substrate, which can be regarded as colloid-based growth and solution-based growth separately (see the yellow and white contours). Parts C and D of Figure 5 show the colloid-based growth and solution based growth in more detail without the top 1D structure through the TEM images. One can see that the final product also has two different size distributions. Colloid-based growth can be regarded to yield a large hexagonal disk up to ca. 300 nm in size, and solution-based growth produces ca. 10 nm species of perovskite. The species can be embedded in the large disk from HRTEM during the calcination (see Figure 5D, circles). Therefore, the colloidal transformation decisively affects the film morphology of perovskite.

After this colloidal understanding, the perovskite thin films engineered by thermal leaching of excessive organic component and tempering (Figures S4 and S5, Supporting Information) were characterized by XRD to gauge the phase quality. For the CH_3NH_3I-deficient system (0.5:1), the unreacted PbI_2 can be identified from the (001), (002), (003), and (004) peaks at 12.65°, 26.51°, 37.79°, and 51.50°[44] (Figure 6A, 0.5:1, pure

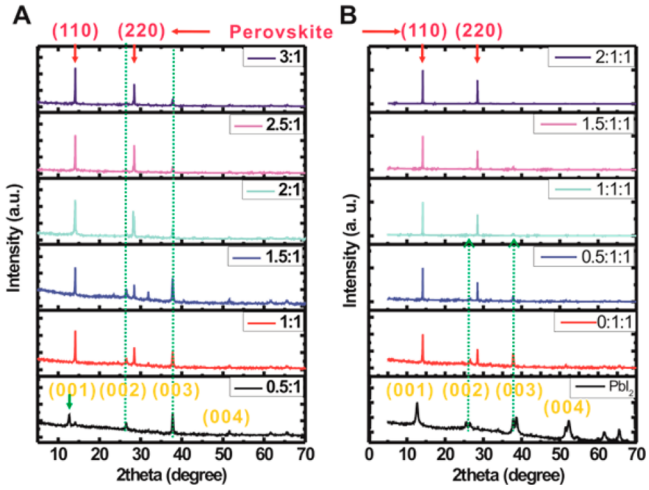

Figure 6. Role of chlorine in phase purity: XRD patterns of the perovskite film using CH_3NH_3I coordination engineering (A) and CH_3NH_3Cl coordination engineering (B).

PbI_2 shown in Figure 6B). In the stoichiometric system (1:1), PbI_2 can still be judged from the (002), (003), and (004) peaks (Figure 6A, 1:1), which means that the 1D structure is PbI_2-impure perovskite, not only morphologically 1D, but also phase-impure. In the engineered systems with excessive methylammonium halide over the stoichiometric ratio, the main diffraction peaks, assigned to the (110) and (220) peaks of $CH_3NH_3PbI_3$ at 14.12° and 28.44°, respectively, are in identical positions for both CH_3NH_3I and CH_3NH_3Cl coordination engineered films, indicating that both techniques have produced the same perovskite thin films in the tetragonal structure. Although both CH_3NH_3I and CH_3NH_3Cl coordination engineering can achieve full and even coverage of perovskite thin films on a planar substrate and produce the same perovskite phase, the phase quality is quite different. CH_3NH_3I coordination engineering suffers from an uncontrolled presence of the nanoscale phase of PbI_2 in the perovskite film during the transformation process, from the appearance of high-energy surfaces of PbI_2 (high-index faceted (003) and (004) planes) and the absence of a low-energy (001) facet.[45] However, CH_3NH_3Cl coordination engineering facilitates the elimination of the PbI_2 impurity through accelerating nucleation and full coordination, as well as the organic impurity by facile and selective release of CH_3NH_3Cl through the large interplanar spacing aforementioned at lower temperature (see Figure S6, Supporting Information), leading to a higher purity of the perovskite film. Although CH_3NH_3Cl was previously employed to assist the film formation,[18−21] the engineering of perovskite toward high purity is first achieved in the present investigation owing to mechanistic understanding of colloidal formation and coordination engineering of the colloidal shape, as well as additional tempering of the perovskite films. Therefore, we accurately identify that excess organic component can tune the size and shape of the coordination

DOI: 10.1021/jacs.5b00321
J. Am. Chem. Soc. 2015, 137, 4460−4468

colloid in relation to the final perovskite grain and particularly partial chlorine substitution can accelerate the crystalline nucleation, induce a layered intermediate phase, and enhance the perovskite coverage, rendering high-quality perovskite films.

Colloid-Processed Photovoltaics. On the basis of as-prepared thin films (Figures S4 and S5, Supporting Information), the solar cells were assembled and the performance parameters were evaluated. The $J-V$ curves as well as dark currents of the different recipes scanned in the forward bias direction and reverse bias direction are shown in Figure 7, and

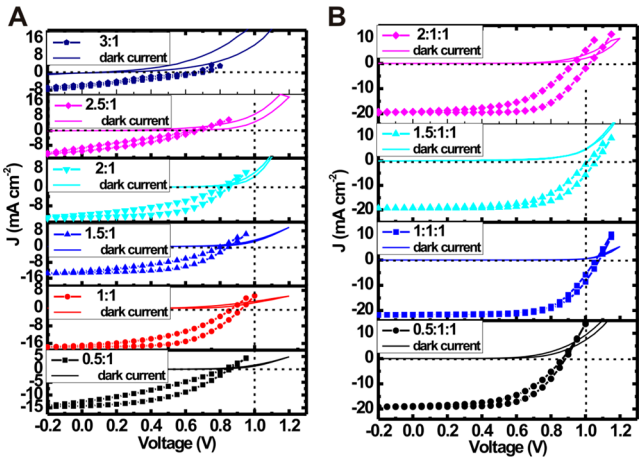

Figure 7. $J-V$ characteristics of the perovskite film using CH_3NH_3I coordination engineering (A) and CH_3NH_3Cl coordination engineering (B) with forward scan and reverse scan directions.

the basic performance parameters are listed in Table S1 (Supporting Information). First, we generally discuss $J-V$ hysteresis in the dark and under illumination. In the dark, PbI_2-rich systems (0.5:1, 1:1) seem to have negligible $J-V$ hysteresis compared to CH_3NH_3I-rich systems (2.5:1, 3:1) (see Figure 7A, dark current), from which we can deduce the excess of organic component is responsible for major hysteresis. Under illumination, the $J-V$ hysteresis can be observed in all systems in Figure 7A; thereby, PbI_2 also causes hysteresis under illumination probably due to defective trapping activated by illumination. Therefore, we can conclude that if a high-quality perovskite film can be achieved, the hysteresis will be eliminated because trapped states are swept away.[46,47] This claim is consistent with the fact that perovskite itself is an excellent photovoltaic material, and therefore, the purer, the better. Then we continue to discuss the $J-V$ performance under illumination in more detail. A 1:1 combination of CH_3NH_3I/PbI_2 is the standard stoichiometric ratio, yielding V_{oc} = 0.932 V, J_{sc} = 17.50 mA cm^{-2}, and FF = 0.555 in the reverse scan and V_{oc} = 0.871 V, J_{sc} = 16.86 mA cm^{-2}, and FF = 0.433 in the forward scan, with PCE amounting to 9.05% and 6.36%, respectively. This is not a good performance, and also a large $J-V$ hysteresis is clearly observed, which can be associated with the presence of PbI_2. The nonstoichiometric combination (0.5:1) of CH_3NH_3I/PbI_2 produces even lower performance; that is, V_{oc} = 0.860 V, J_{sc} = 14.26 mA cm^{-2}, and FF = 0.441, with overall PCE = 5.41% in the reverse scan, and V_{oc} = 0.821 V, J_{sc} = 12.63 mA cm^{-2}, and FF = 0.329, with overall PCE = 3.31% in the forward scan, which can be attributed to a larger excess of PbI_2 in the perovskite films. Although excess CH_3NH_3I coordination can engineer the film coverage, the performance cannot reach a high level due to both CH_3NH_3I residues and the decomposition of $CH_3NH_3PbI_3$ to PbI_2 during the thermal leaching of excess CH_3NH_3I. CH_3NH_3Cl coordination engineering resolved this intractable problem. CH_3NH_3Cl coordination not only engineers the film coverage and crystal orientation, but also ensures the high quality of perovskite crystals themselves owing to facile and selective release of excess CH_3NH_3Cl at low temperature (100 °C). Therefore, despite the small amount of CH_3NH_3Cl, 0.5:1:1 $CH_3NH_3Cl/CH_3NH_3I/PbI_2$ produces V_{oc} = 0.883 V, J_{sc} =

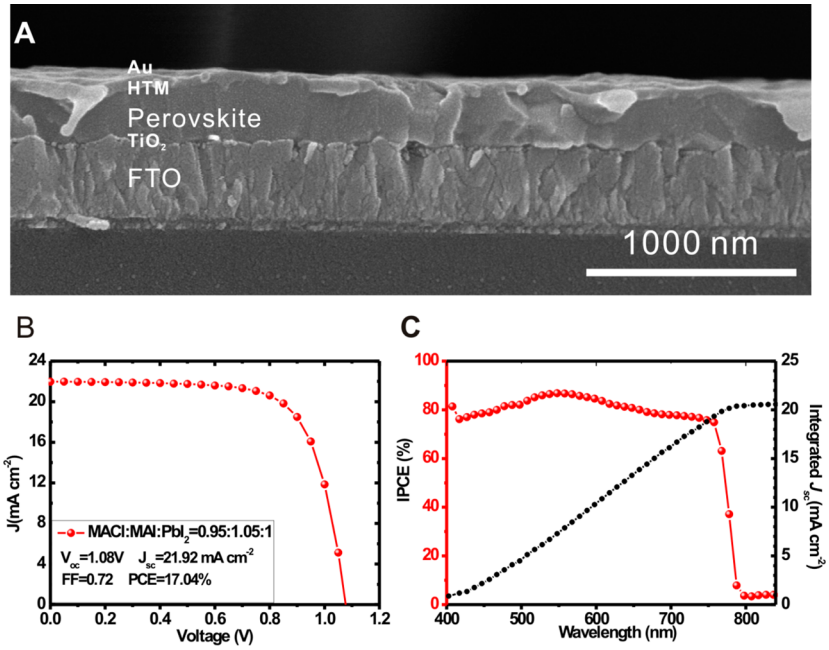

Figure 8. (A) Cross-section SEM image of the best performing solar cell. (B) Optimal $J-V$ performance of coordination engineering (0.95:1.05:1). (C) Under optimal coordination engineering (0.95:1.05:1), IPCE spectrum (red circles and line) and integrated photocurrent density J_{sc} (black line and circles) for the best performing PSC. Integrated J_{sc} was calculated to be 20.61 mA cm^{-2}.

DOI: 10.1021/jacs.5b00321
J. Am. Chem. Soc. 2015, 137, 4460−4468

19.10 mA cm^{-2}, and FF = 0.610 in the reverse scan and V_{oc} = 0.866 V, J_{sc} = 18.86 mA cm^{-2}, and FF = 0.531 in the forward scan, with PCE amounting to 10.30% and 8.67%, respectively, which are much higher than those of the 1:1 recipe. The performance is improved but is still not good due to the partial coverage and also impurity (see Figure 6B). Through the continued addition of CH_3NH_3Cl, 1:1:1 CH_3NH_3Cl/CH_3NH_3I/PbI_2 approaches an optimum, which actually produces V_{oc} = 1.08 V, J_{sc} = 21.63 mA cm^{-2}, and FF = 0.653 in the reverse scan and V_{oc} = 1.06 V, J_{sc} = 21.63 mA cm^{-2}, and FF = 0.643 in the forward scan, with PCEs of 15.29% and 14.75%, respectively, and a mean PCE of 15.01%. This optimal performance should arise from perfect coverage (Figure 3D), the high-purity perovskite phase (Figure 6B) through facile release of excess CH_3NH_3Cl (Figure 4D), a small number of crystalline boundaries (Figure 3D) due to intercrystalline fusion, and so on (see Figure 3D, 1:1:1). A further increase in CH_3NH_3Cl will decrease the performance and especially the photocurrent. More specifically, the 1.5:1:1 CH_3NH_3Cl/CH_3NH_3I/PbI_2 combination produces V_{oc} = 1.07 V, J_{sc} = 19.29 mA cm^{-2}, and FF = 0.633 in the reverse scan and V_{oc} = 1.02 V, J_{sc} = 19.08 mA cm^{-2}, and FF = 0.579 in the forward scan, with PCE amounting to 13.06% and 11.26%, respectively, with a mean PCE of 12.16%. The reduced photocurrent can be explained by the smaller grain size induced by more nuclei of $PbCl_2$, the smaller colloidal size, and more crystal boundaries generated by the release of excess CH_3NH_3Cl (Figure 3D, 1.5:1:1). At last, the 2:1:1 combination of CH_3NH_3Cl/CH_3NH_3I/PbI_2 produces V_{oc} = 1.03 V, J_{sc} = 19.33 mA cm^{-2}, and FF =0.650 in the reverse scan and V_{oc} = 0.93 V, J_{sc} = 19.16 mA cm^{-2}, and FF = 0.525 in the forward scan, with PCE amounting to 12.95% and 9.35%, respectively, with a mean PCE of 11.15%. This can be attributed to pinholes in the film induced by the release of twice the amount of excess CH_3NH_3Cl.

Right now we are definitely confident that the high purity is responsible for the excellent performance without hysteresis. Given that there is still some incident loss of CH_3NH_3I during the thermal leaching of a large amount of CH_3NH_3Cl, for the best performance, further coordination engineering was specially performed, and we have obtained an optimum ratio of 1:1.05:0.95 for CH_3NH_3Cl/CH_3NH_3I/PbI_2. The cross-section SEM image of the engineered solar cell device in Figure 8A shows that the thickness of the perovskite active layer is about 320 nm and the top has a rough morphology full of convex−concave structures using the ultrathin hole-transporting material (HTM) layer, which can induce an optical cavity to enhance J_{sc}.[48] As shown in Figure 8B, it produces V_{oc} = 1.08 V, indeed high J_{sc} = 21.92 mA cm^{-2}, and FF = 0.72, with PCE amounting to 17.04%. The integrated J_{sc} of 20.61 mA cm^{-2} from incident photon-to-electron conversion efficiency (IPCE) data agrees well with the measured value (Figure 8C). To the best of our knowledge, this strikingly high PCE of 17.04% is among the highest PCE in the solution-processed planar version of PSCs. It is noted that perovskite with a small thickness can also afford a large photocurrent thanks to the full coverage. Therefore, this coordination engineering has addressed the intractable coverage problem through the colloidal solution process, along with the high-purity phase brought about, achieving high efficiency comparable to that of the vacuum-deposition process.[6,48]

CONCLUSION

In summary, we investigated the colloidal chemistry of the perovskite precursor solution on the basis of optical spectra and performed coordination engineering to tune the colloidal size and shape for high-quality film coverage, as well as thermal leaching in association with tempering for high crystalline purity, leading to a PCE as high as 17% among PSCs in planar configuration. The organic component plays a crucial role in coordination with the inorganic component in colloidal solution and thereby actually determines the final perovskite quality (namely, morphology, grain size, purity, and crystallinity). 1D structures that interfere with the formation of flat films are effectively eliminated with the aid of judicious colloidal understanding and coordination engineering by utilizing excess methylammonium halide. Perovskite purity, which is highly responsible for the hysteresis of the J−V curve, is elaborately achieved by fast crystallization of $PbCl_2$ nuclei and thermal leaching of excess methylammonium chloride. Our study addresses the fundamental chemistry of the perovskite precursor and provides a generic guideline for accurately controlling the thin-film quality of hybrid perovskite materials, heralding a meaningful avenue for the chemical reactions in terms of materials processing.

ASSOCIATED CONTENT

Supporting Information

Optical images of Tyndall effects of the colloidal solution, perovskite colloidal analysis, optical images and SEM images of perovskite films by CH_3NH_3I coordination engineering and CH_3NH_3Cl coordination engineering, and thermal gravimetric analysis of CH_3NH_3X (X = Cl, Br, I). This material is available free of charge via the Internet at http://pubs.acs.org.

AUTHOR INFORMATION

Corresponding Authors

*yankeyou@gmail.com
*chsyang@ust.hk
*jbxu@ee.cuhk.edu.hk

Author Contributions

§K.Y., M.L., and T.Z. contributed equally to this work.

Notes

The authors declare no competing financial interest.

ACKNOWLEDGMENTS

This work was in part supported by the Research Grants Council and Innovation and Technology Fund of Hong Kong, particularly via Grants T23-407/13-N, ITS/004/14, and HKUST 606511 and 605710 and the CUHK Group Research Scheme.

REFERENCES

(1) Kim, H. S.; Lee, C. R.; Im, J. H.; Lee, K. B.; Moehl, T.; Marchioro, A.; Moon, S. J.; Humphry-Baker, R.; Yum, J. H.; Moser, J. E.; Gratzel, M.; Park, N. G. *Sci. Rep.* **2012**, *2*, 591.

(2) Burschka, J.; Pellet, N.; Moon, S. J.; Humphry-Baker, R.; Gao, P.; Nazeeruddin, M. K.; Gratzel, M. *Nature* **2013**, *499*, 316.

(3) Qiu, J. H.; Qiu, Y. C.; Yan, K. Y.; Zhong, M.; Mu, C.; Yan, H.; Yang, S. H. *Nanoscale* **2013**, *5*, 3245.

(4) Lee, M. M.; Teuscher, J.; Miyasaka, T.; Murakami, T. N.; Snaith, H. J. *Science* **2012**, *338*, 643.

(5) Ball, J. M.; Lee, M. M.; Hey, A.; Snaith, H. J. *Energy Environ. Sci.* **2013**, *6*, 1739.

(6) Liu, M. Z.; Johnston, M. B.; Snaith, H. J. *Nature* **2013**, *501*, 395.

DOI: 10.1021/jacs.5b00321
J. Am. Chem. Soc. 2015, 137, 4460−4468

(7) Heo, J. H.; Im, S. H.; Noh, J. H.; Mandal, T. N.; Lim, C. S.; Chang, J. A.; Lee, Y. H.; Kim, H. J.; Sarkar, A.; Nazeeruddin, M. K.; Gratzel, M.; Seok, S. I. *Nat. Photonics* **2013**, *7*, 487.
(8) Jeon, N. J.; Lee, H. G.; Kim, Y. C.; Seo, J.; Noh, J. H.; Lee, J.; Seok, S. I. *J. Am. Chem. Soc.* **2014**, *136*, 7837.
(9) Wei, Z.; Yan, K.; Chen, H.; Yi, Y.; Zhang, T.; Long, X.; Li, J.; Zhang, L.; Wang, J.; Yang, S. *Energy Environ. Sci.* **2014**, *7*, 3326.
(10) Wei, Z.; Chen, H.; Yan, K.; Yang, S. *Angew. Chem., Int. Ed.* **2014**, *53*, 13239.
(11) Edri, E.; Kirmayer, S.; Mukhopadhyay, S.; Gartsman, K.; Hodes, G.; Cahen, D. *Nat. Commun.* **2014**, *5*, 3461.
(12) Xing, G. C.; Mathews, N.; Sun, S. Y.; Lim, S. S.; Lam, Y. M.; Gratzel, M.; Mhaisalkar, S.; Sum, T. C. *Science* **2013**, *342*, 344.
(13) Stranks, S. D.; Eperon, G. E.; Grancini, G.; Menelaou, C.; Alcocer, M. J. P.; Leijtens, T.; Herz, L. M.; Petrozza, A.; Snaith, H. J. *Science* **2013**, *342*, 341.
(14) Edri, E.; Kirmayer, S.; Henning, A.; Mukhopadhyay, S.; Gartsman, K.; Rosenwaks, Y.; Hodes, G.; Cahen, D. *Nano Lett.* **2014**, *14*, 1000.
(15) Jeon, N. J.; Noh, J. H.; Kim, Y. C.; Yang, W. S.; Ryu, S.; Il Seol, S. *Nat. Mater.* **2014**, *13*, 897.
(16) Im, J.-H.; Jang, I.-H.; Pellet, N.; Grätzel, M.; Park, N.-G. *Nat. Nanotechnol.* **2014**, *9*, 927.
(17) Zhou, H. P.; Chen, Q.; Li, G.; Luo, S.; Song, T. B.; Duan, H. S.; Hong, Z. R.; You, J. B.; Liu, Y. S.; Yang, Y. *Science* **2014**, *345*, 542.
(18) Zhao, Y. X.; Zhu, K. *J. Phys. Chem. C* **2014**, *118*, 9412.
(19) Zhao, Y. X.; Zhu, K. *J. Am. Chem. Soc.* **2014**, *136*, 12241.
(20) Zhao, Y. X.; Nardes, A. M.; Zhu, K. *J. Phys. Chem. Lett.* **2014**, *5*, 490.
(21) Zhao, Y. X.; Nardes, A. M.; Zhu, K. *Appl. Phys. Lett.* **2014**, *104*, 213906.
(22) Zhao, Y. X.; Zhu, K. *J. Phys. Chem. Lett.* **2013**, *4*, 2880.
(23) Qin, P.; Tanaka, S.; Ito, S.; Tetreault, N.; Manabe, K.; Nishino, H.; Nazeeruddin, M. K.; Gratzel, M. *Nat. Commun.* **2014**, *5*, 4838.
(24) Qin, P.; Paek, S.; Dar, M. I.; Pellet, N.; Ko, J.; Gratzel, M.; Nazeeruddin, M. K. *J. Am. Chem. Soc.* **2014**, *136*, 8516.
(25) Qin, P.; Kast, H.; Nazeeruddin, M. K.; Zakeeruddin, S. M.; Mishra, A.; Bauerle, P.; Gratzel, M. *Energy Environ. Sci.* **2014**, *7*, 2981.
(26) Pellet, N.; Gao, P.; Gregori, G.; Yang, T. Y.; Nazeeruddin, M. K.; Maier, J.; Gratzel, M. *Angew. Chem., Int. Ed.* **2014**, *53*, 3151.
(27) Gratzel, M. *Nat. Mater.* **2014**, *13*, 838.
(28) Gao, P.; Gratzel, M.; Nazeeruddin, M. K. *Energy Environ. Sci.* **2014**, *7*, 2448.
(29) Noel, N. K.; Stranks, S. D.; Abate, A.; Wehrenfennig, C.; Guarnera, S.; Haghighirad, A. A.; Sadhanala, A.; Eperon, G. E.; Pathak, S. K.; Johnston, M. B.; Petrozza, A.; Herz, L. M.; Snaith, H. J. *Energy Environ. Sci.* **2014**, *7*, 3061.
(30) Leijtens, T.; Lauber, B.; Eperon, G. E.; Stranks, S. D.; Snaith, H. J. *J. Phys. Chem. Lett.* **2014**, *5*, 1096.
(31) Eperon, G. E.; Burlakov, V. M.; Docampo, P.; Goriely, A.; Snaith, H. J. *Adv.Funct. Mater.* **2014**, *24*, 151.
(32) Burlakov, V. M.; Eperon, G. E.; Snaith, H. J.; Chapman, S. J.; Goriely, A. *Appl. Phys. Lett.* **2014**, *104*, 091602.
(33) Snaith, H. J. *J. Phys. Chem. Lett.* **2013**, *4*, 3623.
(34) Wu, Y. Z.; Islam, A.; Yang, X. D.; Qin, C. J.; Liu, J.; Zhang, K.; Peng, W. Q.; Han, L. Y. *Energy Environ. Sci.* **2014**, *7*, 2934.
(35) Liu, J.; Wu, Y. Z.; Qin, C. J.; Yang, X. D.; Yasuda, T.; Islam, A.; Zhang, K.; Peng, W. Q.; Chen, W.; Han, L. Y. *Energy Environ. Sci.* **2014**, *7*, 2963.
(36) Stamplecoskie, K. G.; Manser, J. S.; Kamat, P. V. *Energy Environ. Sci.* **2015**, *8*, 208.
(37) Tidhar, Y.; Edri, E.; Weissman, H.; Zohar, D.; Hodes, G.; Cahen, D.; Rybtchinski, B.; Kirmayer, S. *J. Am. Chem. Soc.* **2014**, *136*, 13249.
(38) Yan, K. Y.; Xue, Q. Z.; Zheng, Q. B.; Hao, L. Z. *Nanotechnology* **2007**, *18*, 255705.
(39) Yan, K. Y.; Zhang, L. X.; Kuang, Q.; Wei, Z. H.; Yi, Y.; Wang, J. N.; Yang, S. H. *ACS Nano* **2014**, *8*, 3771.
(40) Yan, K. Y.; Zhang, L. X.; Qiu, J. H.; Qiu, Y. C.; Zhu, Z. L.; Wang, J. N.; Yang, S. H. *J. Am. Chem. Soc.* **2013**, *135*, 9531.
(41) Mosconi, E.; Amat, A.; Nazeeruddin, M. K.; Gratzel, M.; De Angelis, F. *J. Phys. Chem. C* **2013**, *117*, 13902.
(42) Xiao, Z.; Bi, C.; Shao, Y.; Dong, Q.; Wang, Q.; Yuan, Y.; Wang, C.; Gao, Y.; Huang, J. *Energy Environ. Sci.* **2014**, *7*, 2619.
(43) Bi, C.; Shao, Y.; Yuan, Y.; Xiao, Z.; Wang, C.; Gao, Y.; Huang, J. *J. Mater. Chem. A* **2014**, *2*, 18508.
(44) Gulia, V.; Vedeshwar, A. G. *Phys. Rev. B* **2007**, *75*, 045409.
(45) Tian, N.; Zhou, Z. Y.; Sun, S. G.; Ding, Y.; Wang, Z. L. *Science* **2007**, *316*, 732.
(46) Shao, Y. H.; Xiao, Z. G.; Bi, C.; Yuan, Y. B.; Huang, J. S. *Nat. Commun.* **2014**, *5*, 5784.
(47) Wang, Q.; Shao, Y. C.; Dong, Q. F.; Xiao, Z. G.; Yuan, Y. B.; Huang, J. S. *Energy Environ. Sci.* **2014**, *7*, 2359.
(48) Lin, Q.; Armin, A.; Nagiri, R. C. R.; Burn, P. L.; Meredith, P. *Nat. Photonics* **2015**, *9*, 106.

DOI: 10.1021/jacs.5b00321
J. Am. Chem. Soc. 2015, 137, 4460−4468